ROYAL SOCIETY OF CHEMISTRY

Check for updates

TiO$_2$/graphitic carbon nitride nanosheet composite with enhanced sensitivity to atmospheric water†

Tosapol Maluangnont, [iD] *[a] Phieraya Pulphol,[b] Satana Pongampai,[c] Thawanrat Kobkeatthawin,[d] Siwaporn Meejoo Smith [iD] [d] and Naratip Vittayakorn[c]

Understanding the fundamentals of transport properties in two-dimensional (2D) materials is essential for their applications in devices, sensors, and so on. Herein, we report the impedance spectroscopic study of carbon nitride nanosheets (CNNS) and the composite with anatase (TiO$_2$/CNNS, 20 atom% Ti), including their interaction with atmospheric water. The samples were characterized by X-ray diffraction, N$_2$ adsorption/desorption, solid state ^{1}H nuclear magnetic resonance spectroscopy, thermogravimetric analysis, and transmission electron microscopy. It is found that CNNS is highly insulating (resistivity $\rho \sim 10^{10}$ Ω cm) and its impedance barely changes during a 20 min-measurement at room temperature and 70% relative humidity. Meanwhile, incorporating the semiconducting TiO$_2$ nanoparticles ($\sim$10 nm) reduces ρ by one order of magnitude, and the decreased ρ is proportional to the exposure time to atmospheric water. Sorbed water shows up at low frequency ($<10^2$ Hz) with relaxation time in milliseconds, but the response intrinsic to CNNS and TiO$_2$/CNNS is evident at higher frequency ($>10^4$ Hz) with relaxation time in microseconds. These two signals apparently correlate to the endothermic peak at $\leq$110 °C and >250 °C, respectively, in differential scanning calorimetry experiments. Universal power law analysis suggests charge hopping across the 3D conduction pathways, consistent with the capacitance in picofarad typical of grain response. Our work demonstrates that the use of various formalisms (*i.e.*, impedance, permittivity, conductivity, and modulus) combined with a simple universal power law analysis provides insights into water-induced transport of the TiO$_2$/CNNS composite without complicated curve fitting procedure or dedicated humidity control.

Introduction

Graphitic carbon nitrides (g-C$_3$N$_4$) are defect-rich, polymeric aromatic layered materials consisting mainly of C and N atoms bonded in sp^2 fashion. The parallel chains of tri-*s*-triazine units organize in layers with A–B stacking, together with a misalignment to decrease the repulsive π–π interactions.[1] Moreover, stacks of graphitic layers can be separated into carbon nitride nanosheets (CNNS) by a facile thermal exfoliation.[2] These nanosheets can be further modified by compositing with metals[3,4] or metal oxides,[5] leading to potential applications in

photocatalysis,[2,6,7] thermal catalysis,[4] optical sensing,[8] nanocomposites,[9] to name but a few.

While the electronics properties of g-C$_3$N$_4$-based materials are widely investigated, the fundamentals of their electrical properties are less well known, contrasting with closely related materials such as amorphous carbon[10] or amorphous carbon nitride.[11–13] The studies on g-C$_3$N$_4$ and/or CNNS focus on thin film devices[14–20] including diode, double dielectric, metal–insulator–semiconductor, typically prepared by sophisticated vacuum techniques. It is known that the electrical conductivity of g-C$_3$N$_4$ along the basal plane (*i.e.* in plane) is approximately two orders of magnitude smaller than that through the stacked layers (out of plane).[21] A few authors explored the properties of g-C$_3$N$_4$-based composites with metal oxides or polymers,[22–25] where the tested specimens can be easily prepared by pelletizing the powder. It was found that the dielectric permittivity ε' of g-C$_3$N$_4$ varies from 7 in thin film[13,18] to $\sim$60 in bulk.[23,24] Pareek and Quamara[24] showed the decreasing ε' with increasing TiO$_2$ content in the TiO$_2$/g-C$_3$N$_4$ composite, despite of the intrinsic dielectric nature of TiO$_2$. Moreover, ε' of BaTiO$_3$/g-C$_3$N$_4$ composite is even lower than the individual components.[23] Meanwhile, Liu *et al.*[25] reported that the addition of g-C$_3$N$_4$ increased ε' of the composite based on poly(vinylidene fluoride).

[a]*Electroceramics Research Laboratory, College of Materials Innovation and Technology, King Mongkut's Institute of Technology Ladkrabang, Bangkok 10520, Thailand. E-mail: tosapol.ma@kmitl.ac.th*

[b]*Department of Materials Science, Faculty of Science, Srinakharinwirot University, Bangkok 10110, Thailand*

[c]*Advanced Materials Research Unit and Department of Chemistry, School of Science, King Mongkut's Institute of Technology Ladkrabang, Bangkok 10520, Thailand*

[d]*Center of Sustainable Energy and Green Materials and Department of Chemistry, Faculty of Science, Mahidol University, Nakhon Pathom 73170, Thailand*

Specifically, TiO_2/CNNS composite is widely studied for organic disinfection in water because the heterojunction tailors band structure and charge separation.[2,26,27] In this regard, water adsorption on surface is an important microscopic process in *e.g.*, photocatalysis, sensors, and separation membranes.[28] The sensitivity to atmospheric water leads to such applications, but it also complicates fundamental understanding of charge transport. Examples of materials exhibiting proton conduction are layered double hydroxides,[29] titanate nanowires/nanotubes,[30,31] illitic clay,[32] and TiO_2.[33,34] For g-C_3N_4, water dissociates at the defect site and forms a mixed adsorption structure including a hydroxy group.[35] A single layer of CNNS is an indirect semiconductor with the calculated band gap energy of 1.15–2.72 eV.[36] Upon water adsorption, the sheet becomes buckled, and the band gap is direct with the band gap energy increasing to 1.79–3.05 eV. The calculated adsorption energy[36] is larger than that on graphene and comparable to that on metal oxides, suggesting favorable water adsorption. Such water-induced charge transport explains the use of g-C_3N_4- or CNNS-based devices for humidity detection,[14,15,22,37,38] where the resistance/impedance, capacitance, optical transmitted power, current, *etc.*, were measured at varying relative humidity. However, the scarcity of studies on water-induced electrical properties of the TiO_2/CNNS composite contrasts with the known surface protonic conduction and surface–water interactions in TiO_2 (ref. 33, 34 and 39) or g-C_3N_4 and CNNS.[35,36]

Impedance spectroscopy is an important tool to elucidate the nature of charge transport in materials ranging from ionic to insulator, from crystalline to amorphous, from organic to inorganic, and so on.[40,41] The alternating current (AC) responses are described in four basic formalisms including complex impedance Z^*, complex admittance Y^* (or conductivity σ^*), complex permittivity ε^*, and complex electric modulus M^*. In particular, the frequency dependence of σ^* and ε^* follows the universal power law proposed by Jonscher,[42–44] which provide further insights into effective dimensionality of charge transport. Herein, we report the impedance study of TiO_2/CNNS composite and CNNS, supplemented by the direct current–voltage (*I–V*) measurement, in a simple time-dependent experimental set up and sample pretreatments without the need for dedicated humidity control. The samples were characterized by X-ray diffraction (XRD), N_2 adsorption/desorption, solid state ^{1}H nuclear magnetic resonance spectroscopy (^{1}H NMR), thermogravimetric analysis (TGA), differential scanning calorimetry (DSC), and transmission electron microscopy (TEM). Our work contributes to the understanding of fundamental AC electrical properties in TiO_2/CNNS or CNNS, including those induced by atmospheric water, such as dielectric permittivity, effective dimensionality of charge carriers, and relaxation time.

Experimental

Synthesis

Bulk graphitic carbon nitride was prepared by a direct heating of urea powder (125 g) in an alumina crucible with a cover at 600 °C (heating rate 10 °C min^{-1}) for 4 h.[2] After cooling down to room temperature (RT), the pale-yellow product was collected

and ground into powder. The nanosheets analog (carbon nitride nanosheets, CNNS) was produced by immersing the bulk powder (2.5 g) in 100 mL of HNO_3 (65%) for 12 h. The obtained sample was filtered and washed with deionized water, and further heated at 500 °C for 4 h.

To prepare the TiO_2/CNNS composite, an amount of 1 g of $TiOSO_4$ was stirred in 100 mL of deionized water for 15 min and sonicated for 20 min.[2] Then, 4 g of CNNS (dispersed in water) was added into this solution. The slurry was further sonicated at RT for 30 min to obtain the homogeneous mixing. The solution was transferred to a Teflon-lined stainless-steel autoclave and heated at 180 °C for 4 h. The product was collected *via* centrifugation, washed with water, and dried at 65 °C for 24 h.

Characterization

XRD was performed using Cu Kα radiation at $2\theta = 10°–60°$ (Bruker model D2 PHASER). The specific surface area S_{BET} was measured *via* N_2 adsorption/desorption using an Autosorb-1C instrument (Quantachrome) after degassing at 300 °C. ^{1}H solid state NMR spectra were acquired using a JEOL 400YH operating at 400 MHz. TGA was performed under the flow of N_2 gas (20 mL min^{-1}) from RT to 800 °C (10 °C min^{-1}) using a PerkinElmer, Pyris-1 instrument. DSC measurements were conducted using a Netzsch DSC 3500 instrument with the sample (≤10 mg) packed inside an Al crucible with pierced lid and an empty Al crucible as a reference, from RT to 400 °C using two heating rates (0.5 and 25 °C min^{-1}). The morphology of the samples was characterized by transmission electron microscopy at 200 kV (JEOL, JEM 2010).

Electrical properties measurements

An amount of ~30 mg of TiO_2/CNNS powder was pressed without a binder into a pellet with thickness of ~0.15 mm and diameter of ~0.5 mm (apparent density of 1.16 g cm^{-3}). On the other hand, the CNNS pellet could be prepared only with at least ~60 mg of the powder, leading to a thicker (~0.3 mm) specimen with an apparent density of 1.04 g cm^{-3}. For comparison, the theoretical density of g-C_3N_4 is 2.34 g cm^{-3}, suggesting porosity in both specimens.

The pellet was gold-sputtered on both sides to form electrical contacts. All measurements were conducted using a precision LCR meter (HP-4284A, Hewlett-Packard, Palo Alto, CA) covering the frequency $f = 20$ to 10^6 Hz. The data were collected under a typical laboratory atmosphere at 25 °C and the relative humidity of ~70% following one or more of these pretreatments/conditions:

(i) "Dry": the pellet was dried at 60 °C for 3 days prior to the immediate impedance measurement at RT. The sample removal from the oven to the start of the measurement typically took less than one minute.

(ii) "Air exposed": the pellet was left under ambient for 2 days prior to the remeasurement at RT, and.

(iii) "400 °C": the air exposed pellet was heated up from 25 to 400 °C (2 °C min^{-1}), stabilized at 400 °C for 15 min, after which the sample impedance was recorded.

In all conditions, up to 8 cycles were repeated during a total time of 20 min. Note that we observed the artefact in our setup at $\sim 10^5$ Hz which is removed from all frequency-dependent plots presented herein.

The direct current–voltage (I–V) characteristics was measured only under condition (i) using an LCR meter (Agilent, E4980A model) and a 0.5 V interval from −10 to 10 V.

Results and discussion

Sample characteristics

Fig. 1a shows the XRD patterns of the two samples. All are typical of g-C$_3$N$_4$ (JCPDS 87-1526) with two prominent peaks at $\sim 27.5°$ and 13.0° due to the stacking of the graphitic carbon nitride sheet and the constituting aromatic tri-s-triazine unit.[1,2] The broad reflections indicate the small number of coherent length along the c-direction (i.e., thickness of the stacked sheets) due to the HNO$_3$-assisted thermal exfoliation.[2] The lack of any TiO$_2$ reflections in the composite suggests that the metal oxide must be extremely small. Fig. 1b show the N$_2$ adsorption/desorption isotherms of the samples. They are classified as type IV characteristics of monolayer adsorption and capillary condensation as evident by the hysteresis at $P/P_0 > 0.5$.[45] The specific surface S_{BET} is similar at 118 m^2 g^{-1} for CNNS, and 113 m^2 g^{-1} for TiO$_2$/CNNS. The ^{1}H NMR spectra in Fig. 1c comprise of three signals at ~ 10.9, 5.8–6.2, and 2.3–2.7 ppm. These chemical shifts are due to H attached to N atom (H_{amine}), H$_2$O (H_W), and H attached to C atom ($H_{aliphatic}$), respectively.[46,47]

Accordingly, the presence of water in both samples is suggested spectroscopically.

In addition, Fig. 1d shows that the samples undergo a mass loss as soon as the temperature is raised, presumably due to the removal of loosely bound, physisorbed water. The loss at $T <$ 200 °C (inset) translates to the water content of 2.1 and 2.7 wt% for CNNS and TiO$_2$/CNNS, respectively. This finding hints at the enhanced hydrophilic nature of the composite. At $T >$ 400 °C, a significant mass loss is observed in both samples, which limits the temperature for electrical properties investigation. Meanwhile, DSC in Fig. 1e shows endothermic peak at ~ 87–89 °C (at the heating rate 0.5 °C min^{-1}) or ~ 103–111 °C (at the heating rate 25 °C min^{-1}), ascribed to the removal of physisorbed water. Another broad, endothermic peak is at >250 °C in both samples which is independent of the heating rate. Notably, the heat flow (i.e., peak area) and peak temperature of TiO$_2$/CNNS are consistently larger than those of CNNS, suggesting a stronger water–surface interaction in the former.

Lastly, morphology of the samples was examined by TEM. Thin sheets with faint contrast as typical with nanosheets are observed for CNNS in Fig. 2a. This feature is preserved in the TiO$_2$/CNNS composite (Fig. 2b and c), which also contains particles of ~ 10 nm on top. The lattice fringe of the nanoparticle corresponding to 0.34 nm agrees with the (101) plane of anatase-type TiO$_2$. Formation of the (101) facet of TiO$_2$ on g-C$_3$N$_4$ has been frequently observed.[48,49] This is because the (101) facet has the lower surface energy (0.44 J m^{-2}) than other surfaces, such as the (001) with the surface energy of

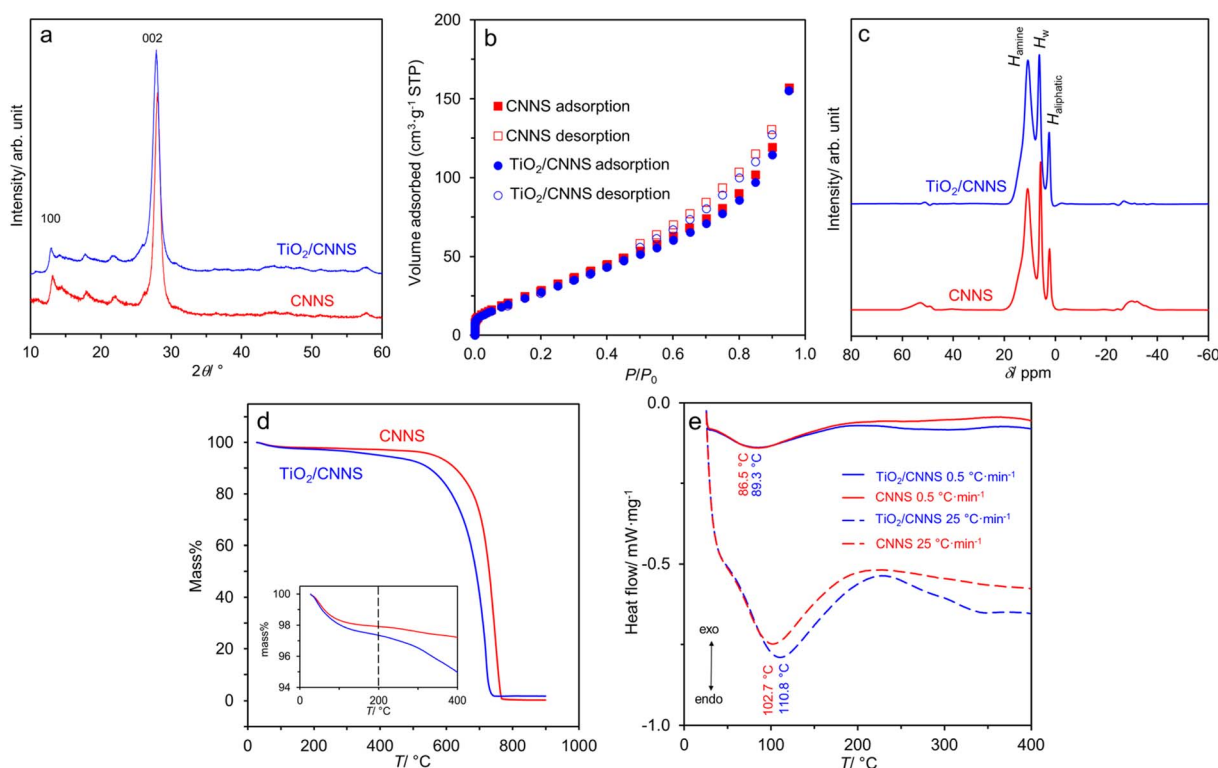**Fig. 1** Some characteristics of CNNS and TiO$_2$/CNNS composite: (a) XRD patterns, (b) N$_2$ adsorption/desorption isotherms, (c) ^{1}H NMR spectra, (d) mass loss curves, and (e) heat flow curves.
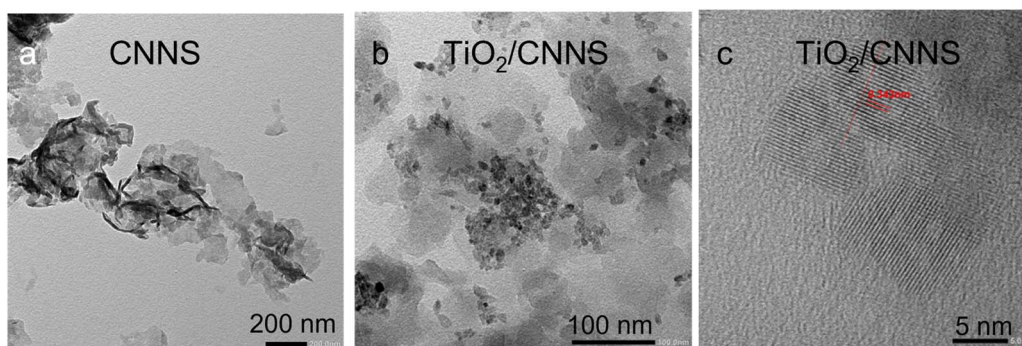
Fig. 2 TEM images of (a) CNNS, and (b and c) TiO$_2$/CNNS. Note the difference in the scale bar.

0.90 J m^{-2}.[50] An energy dispersive X-ray analysis (Fig. S1†) indicates 20 atom% Ti in the composite.

Impedance and direct current measurements

The complex impedance Z^* is described by

$$Z^* = Z' + iZ'' \tag{1}$$

with Z' and Z'' as the real and imaginary part of the function, respectively. Fig. 3a is the Nyquist plots of TiO$_2$/CNNS showing a semicircle which becomes smaller during repeated measurements (initial i, to final f) throughout 20 min. The smaller semicircle translates to the decreasing impedance. Considering the well-known proton conduction in TiO$_2$ (ref. 33 and 34) and g-

C$_3$N$_4$ (or CNNS),[14,15,22,35–38] the present finding might be explained by additional charge carriers generated by water dissociation (i.e., protonic conduction). In a separate experiment, the impedance was measured at 400 °C where the influence of adsorbed water could be excluded. As shown by the filled symbols in the inset of Fig. 3a, the impedance at i and f measurements nicely overlaps not only with each other at 400 °C, but also with data from different repetitions at RT. Apparently, the simple time-dependent measurements demonstrate that atmospheric water contributes to the decreasing impedance of TiO$_2$/CNNS under typical laboratory conditions (25 °C and ~70% relative humidity), but not at 400 °C.

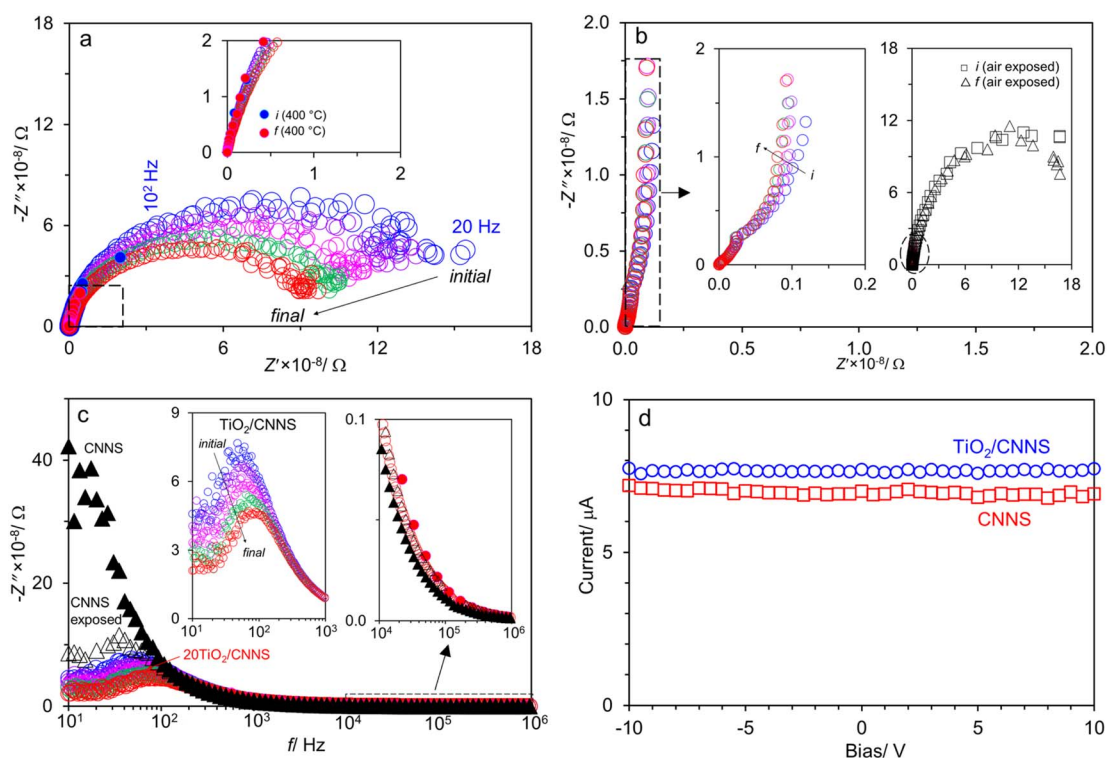Fig. 3b shows that the Nyquist plots of CNNS appear almost as a straight line, indicating that it is highly insulating which is

Fig. 3 The Nyquist plots from impedance measurements of (a) TiO$_2$/CNNS, and (b) CNNS. Panel (c) shows the $-Z''(f)$ plots of the data from the final (f) repetition of the 20 min-measurement. Panel (d) is the $I-V$ plots from the direct current measurement.

consistent with others.[15,18,22,33] Unlike TiO$_2$/CNNS, CNNS shows relatively constant impedance which just slightly moves throughout 20 min (left inset of Fig. 3b), suggesting that CNNS is not as sensitive to atmospheric water as TiO$_2$/CNNS (the direct comparison of impedance in absolute value is not straightforward, however, because the CNNS pellet is thicker).

In another experiment, the CNNS sample was left under ambient for 2 days for exposure to atmospheric water prior to the impedance measurements. The "air exposed" sample now shows a clear semicircle (right inset of Fig. 3b) which remains constant throughout the 20 min-measurement. Meanwhile, the data at high f (left circle on the right inset of Fig. 3b) overlap with those from the dry CNNS. Accordingly, air exposure for a few days (instead of merely 20 min) sufficiently generates water-induced charge carriers in CNNS, thereby decreasing its impedance.

Fig. 3c shows the spectroscopic plots $-Z''(f)$ at the final repetition. In all cases, there is a broad and asymmetric peak with varies in the maximum impedance Z''_{max} and the frequency f_{max} especially on the low frequency side. Otherwise, the data at high f are very similar (see the right inset of Fig. 3c). This finding indicates that the response due to adsorbed water (or water–surface interaction) dominates at low f, while that of materials dominates at high f. Specifically, Z''_{max} of TiO$_2$/CNNS systematically shifts to the higher f and shows the lower Z''_{max} with increasing repetition. The magnitude of Z''_{max} in the order CNNS > CNNS (air exposed) > TiO$_2$/CNNS is inversely proportional to the extent of water-induced conduction.

The resistance R (Ω) and resistivity ρ (Ω cm) can be calculated from Z''_{max}, following eqn (2):

$$R = 2Z''_{max} = \rho t/A \qquad (2)$$

where t is the thickness in cm of the pellet (i.e., the distance between electrodes), and A is the area of the pellet in cm^2. Table 1 summarizes the calculated ρ and the resistance R_{LF} in bracket. (The subscript LF indicates that it appears at low frequency.) CNNS is highly resistive ($\rho \sim 8 \times 10^9$ Ω cm, vs. 10^{13} Ω cm in carbon nitride thin films on silicon[13]). This is explained by a simple specimen pressing which generates many grain boundaries/contact resistance, in addition to the intrinsically insulating nature of CNNS. Exposure to water in the air for two days reduces ρ by a factor of four to $\sim 2 \times 10^9$ Ω cm. Meanwhile,

addition of 20 atom% Ti as the semiconducting TiO$_2$ nanoparticles decreases the resistivity ($\rho \sim 1.1$–1.9×10^9 Ω cm) presumably due to the enhanced charge transfer at the TiO$_2$/CNNS heterojunction.[27] It is widely accepted that electron transfers g-C$_3$N$_4$ to the (101) facet of TiO$_2$ in photocatalysis.[51] However, it is more likely that charges (protons) transport all over the materials in this work (i.e., without the need to consider light absorption), see charge conduction pathway below. The two major proton transport mechanisms are Grotthuss mechanism and vehicle mechanism, but it is too speculative to suggest one over another at present.

Fig. 3d compares the I–V plots performed right after the pellet was removed from the oven. Considering that the measurement was quickly accomplished in 5 min, we assume that the interference by atmospheric water is minimal. The two samples display a relatively constant direct current I over the bias from −10 to 10 V. It is found that I is 7.66(4) μA for TiO$_2$/CNNS, and 6.95(9) μA for CNNS, where the number in parenthesis is the standard deviation to the last digit. Using geometrical surface area of each specimen, the current density is 34.7(2) μA cm^{-2} for TiO$_2$/CNNS and 32.7(4) μA cm^{-2} for CNNS. Recently, Urakami et al.[16,17] reported the direct current on the order of pA (in plane) vs. μA (out of plane) in g-C$_3$N$_4$ thin films. It was explained that carriers are confined around the N atom for the in-plane direction, leading to low conductivity in the pA range. In contrast, delocalized hopping occurs more easily along stacks of sheets, leading to a higher current on the μA range for the out of plane direction.[17,21] The electrical properties reported herein for TiO$_2$/CNNS and CNNS pellets are likely dominated by conduction across the plane, because the graphitic layers were uniaxially pressed to be parallel to others prior to gold sputtering on the opposite faces of the pellet.

Dielectric properties, conductivity, and electric modulus

The complex dielectric permittivity ε^* [eqn (3)] can be calculated from Z' and $-Z''$ following eqn (4) and (5)

$$\varepsilon^* = \varepsilon' + i\varepsilon'' \qquad (3)$$

$$\varepsilon' = (t/\omega A\varepsilon_0)[Z''/(Z'^2 + Z''^2)] \qquad (4)$$

$$\varepsilon'' = (t/\omega A\varepsilon_0)[Z'/(Z'^2 + Z''^2)] \qquad (5)$$

Table 1 The list of ρ, R, C, and τ from different samples and pretreatments/conditions[a,b]

Sample	Pretreatment or condition	ρ/Ω cm [$R_{LF}/G\Omega$]	C_{LF}/pF	C_{MF}/pF	C_{HF}/pF	τ_{LF}/ms	τ_{MF}/μs	τ_{HF}/μs
CNNS	Initial, RT	7.7×10^9 [9.8]	—	5.30	4.19	—, 6.9	78.4, —	9.7, —
	Final, RT	7.7×10^9 [9.8]	—	5.81	4.12	—, 13.8	59.4, —	8.4, —
	Initial, RT (air exposed)	1.7×10^9 [2.2]	3.28	—	4.53	10.5, 5.2	—, —	4.8, —
	Final, RT (air exposed)	1.8×10^9 [2.3]	3.28	—	4.50	10.5, 4.5	—, —	4.2, —
TiO$_2$/CNNS	Initial, RT	1.9×10^9 [1.5]	2.29	—[c]	4.05	13.1, 3.3	—, —	8.7, —
	Final, RT	1.1×10^9 [0.9]	2.31	—	4.02	10.8, 2.3	—, —	7.9, —
	Initial, 400 °C	—	—	—	—	—, —	—, —	1.4, —
	Final, 400 °C	—	—	—	—	—, —	—, —	1.4, —

[a] ρ and R calculated from $-Z''$, C calculated from the M' vs. M'' plot. The relaxation time before comma is τ(tan δ), and that after comma is $\tau(Z'')$. [b] The subscript LF, MF, and HF refer to low-, medium-, and high-frequency, respectively. [c] The symbol — means not detected.

with ε' and ε'' as the real- and imaginary part of the complex dielectric function; t and A is the thickness and area of the pellet in cm and cm^2 respectively; $\omega = 2\pi f$; and ε_0 is the vacuum permittivity (8.854×10^{-12} F m^{-1}).

Fig. 4a compares ε' at the end of the 20 min-measurement, showing two parts. Firstly, ε' very strongly decreases with increasing f (<80 Hz). It is known that water shows high ε' at low f (5×10^5 at ~80 Hz) which rapidly decreases with increasing f (79 at 10^6 Hz).[52] Accordingly, the dielectric response at low f is attributed to sorbed water interacting with the surface, presumably in combination with electrode polarization. This may be correlated to the dominating peak of $-Z''(f)$ in Fig. 3c. Secondly, the variation of ε' becomes modest up to 10^6 Hz and this could be characteristics of water-free materials. The decrease of ε' with increasing f in both regions is expected (see, *e.g.*, ref. 42, 53 and 54) because dipoles cannot effectively reorient themselves with the increasing alternating field.

At $f = 10^6$ Hz, ε' for CNNS, TiO$_2$/CNNS (both at RT) and TiO$_2$/CNNS (400 °C) is practically similar at 10–15, which are smaller than that of the air exposed, water-sorbed CNNS (21). These values might be compared to ε' of 7–8 in graphitic carbon nitride thin films.[13,18] Accordingly, TiO$_2$ promotes only the rate of water uptake, but does not contribute to magnitude of ε', especially when the atmospheric water uptake is already saturated (*i.e.*, at 20 min). The similar ε' without or with added TiO$_2$ was earlier reported in TiO$_2$/g-C$_3$N$_4$ (ref. 24) and BaTiO$_3$/g-C$_3$N$_4$ (ref. 23) composites. This finding was earlier explained by the altered band gap which affects the electronic polarization and

consequently ε'.[23,24] Additionally, ε' of the TiO$_2$/CNNS composite at 400 °C (filled circles in Fig. 3a) is smaller than that at RT (open circles) due to the lack of water-induced charge carriers. The data at RT and 400 °C overlap only at $f > 10^5$ Hz, indicating that the water–surface interaction persists even at 400 °C.

Fig. 4b shows that tan δ ($=\varepsilon''/\varepsilon'$) decreases with increasing f as is common.[42,53,54] At low f, the loss tangent is up to 4 for TiO$_2$/CNNS, and 2 for air exposed CNNS. Otherwise, tan δ is ~0.2 at higher f, which is comparable to carbon nitride films on Si by Konofaos *et al.*[13] The high tan δ at low f indicates that they behave more like a conductor than a dielectric, while the rapid increase at low f suggests the onset of direct current conduction.[41] It is postulated that water sorption leads to a conducting hydrolyzed entity on each grain, forming macroscopic dipoles which interact strongly with each other. On the other hand, CNNS exhibit low tan δ throughout because it is less hydrophilic than TiO$_2$/CNNS.

We calculated the AC conductivity σ'_{AC} (*i.e.*, the real part of complex admittance) using eqn (6) and the results are shown in Fig. 4c:

$$\sigma'_{AC} = (t/A)\left[Z'\Big/\left(Z'^2 + Z''^2\right)\right] = \omega\varepsilon'\varepsilon_0 \tan\delta \qquad (6)$$

It is found that σ' is relatively constant at low f, but increases at high f. This behavior is typical of the phenomenal universal power law as proposed by Jonscher, ascribed to interacting charges/dipoles:[42–44]
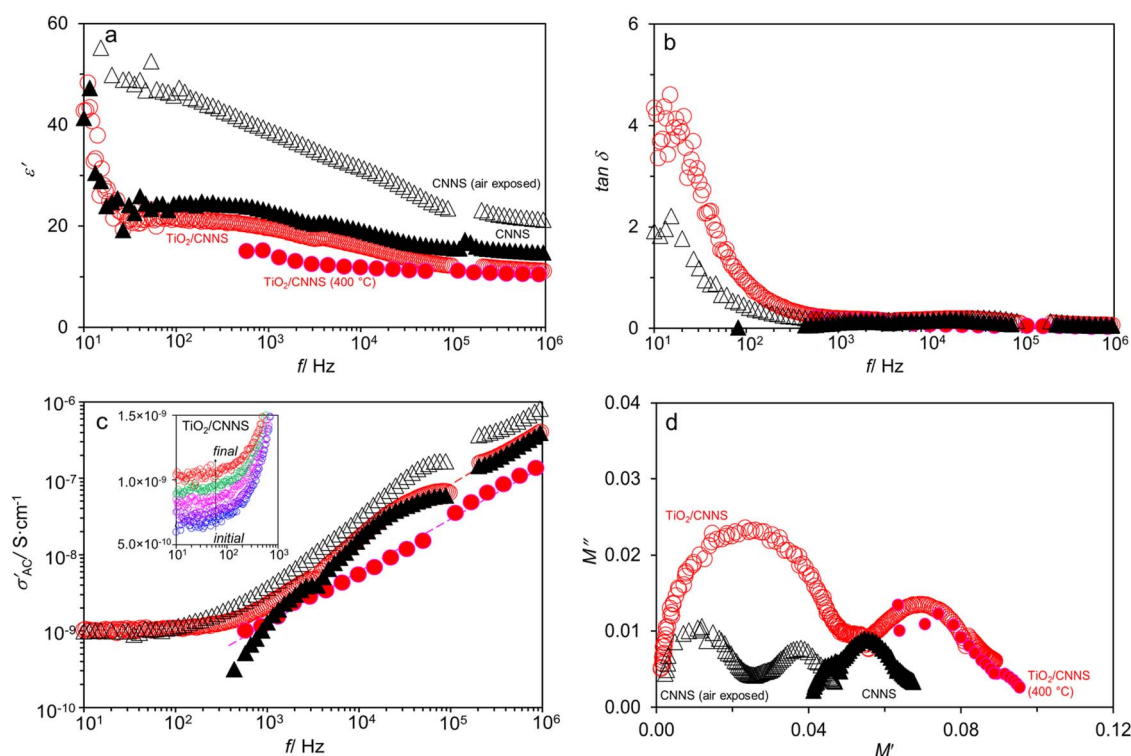

Fig. 4 The frequency dependence of (a) ε', (b) tan δ, (c) σ'_{AC}, and (d) the complex plane plot of the electric modulus M' *vs.* M'', all taken from the final repetition of the 20 min-measurement. The lines in (c) are fit to the Bf^s term in eqn (7). The inset in (c) shows σ'_{AC} at low f for TiO$_2$/CNNS from the initial to final measurements.

$$\sigma'_{AC} = \sigma_{DC} + Bf^s \qquad (7)$$

where σ_{DC} is the frequency-independent intercept, B is the slope, and s is the power. The inset in Fig. 4c shows that σ_{DC} of TiO$_2$/CNNS increases during the 20 min measurement from 6.0×10^{-10} to 1.0×10^{-9} S cm^{-1}. This is clearly the DC conduction. The fitting parameters according to eqn (7) are summarized in Table 2. It is found that the exponent s is 0.65–0.86, close to that in porous titania[39] or layered titanate ceramics.[42] It has been demonstrated[55,56] that s represents the effective dimension of the conduction pathways, with $s > 0.64$ for three-dimensional (3D) one. Hence, the charge/dipole hopping across the 3D conduction pathways can be deduced. This is consistent with the recent simulation of charge transport across the nearest–neighbor transitions in stacks of g-C$_3$N$_4$ by Noda *et al.*[21]

Next, we have calculated the complex electric modulus $M*$ which is the inverse of the complex dielectric permittivity with the real part M' and imaginary part M'' as follows:

$$M* = (1/\varepsilon*) = M' + iM'' \qquad (8)$$

$$M' = \varepsilon'/(\varepsilon'^2 + \varepsilon''^2) \qquad (9)$$

$$M'' = \varepsilon''/(\varepsilon'^2 + \varepsilon''^2) \qquad (10)$$

Fig. 4d shows the complex plane plots of M'–M'' analogous to the Nyquist plots of the impedance. (We deliberately show the unequal x- and y-axis to clearly depict the semicircle.) Two semicircles are evident which contrast with the single semicircle in the Z' *vs.* Z'' plots. Meanwhile, the electric modulus is dominated by electrical components of the smallest capacitance where the maximum value on the y-axis M''_{max} relates to the capacitance C by eqn (11)

$$M''_{max} = C_0/2C \qquad (11)$$

where $C_0 = \varepsilon_0 A/t$.

The calculated capacitance is also shown in Table 1. The C_{LF}, C_{MF}, and C_{HF} correspond to the calculated capacitance at low, middle, and high frequency, respectively. It is found that C varies very slightly (2.3–4.5 pF) despite of the difference in frequency. The capacitances are independent of pretreatment or measurement temperature, and in the order of 10^{-12} F typical of the grain response.[40] The result suggests that adsorbed water covering the grain is bulk-like (but not as the thin/grain

boundary-like layer) and consistent with the 3D conduction as deduced from the exponent s of eqn (7) discussed above.

Relaxation time

A relaxation peak is apparent in the frequency-dependent Z'' (Fig. 3c) and tan δ (Fig. 4b), enabling the calculation of the relaxation time τ as:

$$\tau = 1/(2\pi f_{max}) \qquad (12)$$

where f_{max} is the frequency at the peak maximum. Accordingly, the relaxation time from two formalisms of the same physical process is obtained, $\tau(Z'')$ and $\tau(\tan \delta)$ as also summarized in Table 1. The $\tau(\tan \delta)$ is typically larger than $\tau(Z'')$, consistent with the theoretical explanation.[41]

It is found that τ does not vary appreciably among different samples. At the low-frequency (LF, $f < 80$ Hz), τ_{LF} is ~2–14 ms. While power law analysis indicates a local 3D-hopping, the millisecond-range τ is typical of the relaxation of surface water[57] as opposed to femtoseconds for bulk water.[58] Two other relaxations are observed at middle-frequency (MF, ~10^3 Hz; τ_{MF} = 59–78 μs) and high-frequency (HF, ~10^4 Hz; τ_{HF} = 1–9 μs). It is reasonable assuming that they are characteristics of TiO$_2$/CNNS or CNNS with a minor contribution from adsorbed water. The relaxation time on the μs scale has been reported (or can be deduced) in a closely related amorphous carbon[10] or carbon nitride[12,13] thin films. The two types of relaxation at LF and MF/HF could be linked to the low- and high-temperature endothermic peak in DSC, respectively. The direct comparison between the f-scan experiment and T-scan experiment is not straightforward, however.

Charge conduction pathway

We consider four pathways[28] of water-induced charge transport as schematically depicted in Fig. 5 for TiO$_2$/CNNS. Firstly, the transport at the bulk (I) should be minimal (due to the highly insulating nature[15,18,22,33]) and concentrated mostly in the direction perpendicular to the sheet (*i.e.*, out of plane)[16,17,21] as discussed in the I–V results. On the other hand, the transport along the grain boundary (II) and on the open pores surfaces (III) is possible considering that the samples were simply pressed into pellet, leaving residual porosities. We propose that the adsorbed water in this region is bulk-like, as deduced from the exponent s typical of 3D conduction.[55,56] Lastly, charges could be enriched right below the pore/material interface (IV) presumably as a surface layer. If so, this corresponds to τ_{LF} in milliseconds typical of surface water,[57] as deduced from the relaxation peak in Fig. 3c and 4b.

The protonic conduction of TiO$_2$ is well known, leading to its application as a humidity sensor.[33,34,39] Water molecules accumulated on the surface into different layers which are chemisorbed, ice-like, liquid-like, *etc.*[33] Among different facets, proton conduction on (101) of anatase[33] has a low activation enthalpy because water is loosely bound, as compared to that on (001) and (100) with higher activation enthalpy. As suggested from the time-dependent Nyquist plots of TiO$_2$/CNNS (Fig. 3a),

Table 2 Fitting of the conductivity to the equation $\sigma'_{AC} = \sigma_{DC} + Bf^s$ [eqn (7)]

Sample	Pretreatment or condition	σ_{DC}/S cm^{-1}	B	s
CNNS	Initial, RT	Not observed	7.2×10^{-12}	0.80
	Final, RT	Not observed	4.2×10^{-12}	0.86
	Initial, RT (air exposed)	9.9×10^{-10}	2.0×10^{-11}	0.79
	Final, RT (air exposed)	9.9×10^{-10}	3.9×10^{-11}	0.73
TiO$_2$/CNNS	Initial, RT	6.0×10^{-10}	1.3×10^{-11}	0.76
	Final, RT	1.0×10^{-9}	2.0×10^{-11}	0.73
	Initial, 400 °C	Not observed	1.6×10^{-11}	0.65
	Final, 400 °C	Not observed	1.1×10^{-11}	0.68

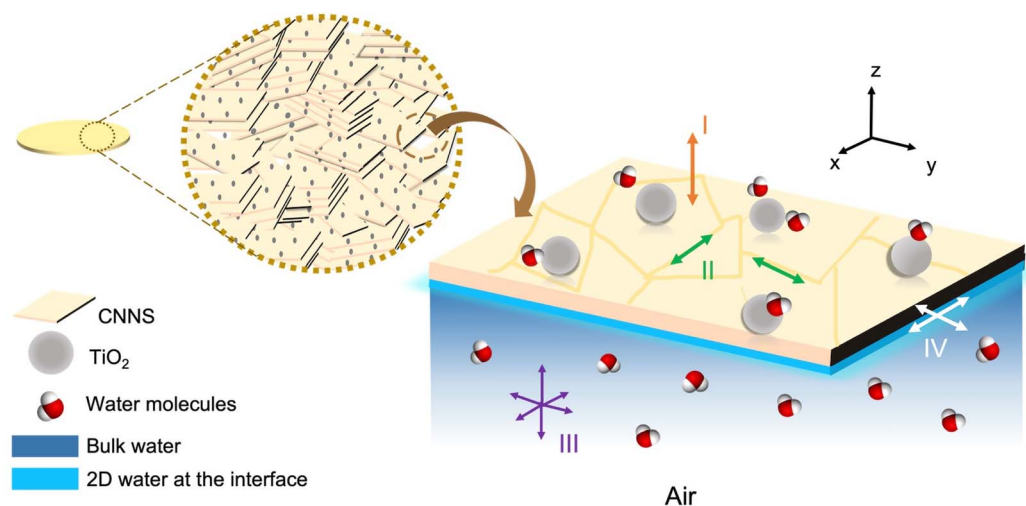**Fig. 5** Schematic diagram of proton conduction in TiO$_2$/CNNS, depicting four charge transport pathways (I to IV).

it is likely that water is preliminarily adsorbed first on the (101) facet of TiO$_2$ nanoparticles which are distributed throughout the composite. The adsorbed water (or proton) then transports to other parts, thereby demonstrating the increased sensitivity to water, presumably *via* the synergistic effect of TiO$_2$.

Conclusions

(1) The TiO$_2$/CNNS composite shows decreasing Z' (and increasing σ'_{AC}) with repetition across the 20 min-measurement at RT and 70% RH, indicating the increased sensitivity to atmospheric water. Simultaneously, $-Z''$ and tan δ show a peak with increasing f (*i.e.*, a decreasing τ). Altogether, proton conduction due to water adsorption and dissociation can be inferred. On the other hand, these signals are not observed at 400 °C and consistent with water loss at elevated temperature deduced from TGA and DSC.

(2) CNNS is highly insulating, but it allows detectable proton conduction given sufficient equilibration to atmospheric water as demonstrated for air exposed CNNS. The ε' of CNNS and TiO$_2$/CNNS (at 10^6 Hz) of $\sim$10–15 is reasonably close to 7 in the previously reported thin film.

(3) The universal power law fitting of $\sigma'_{AC}[= \sigma_{DC} + Bf^s]$ suggests the 3D hopping of charges (*i.e.*, proton conduction), likely reflecting the transport along the grain boundary and the open pores surfaces. Meanwhile, two ranges of the relaxation times are deduced from the frequency dependence of $-Z''$ and tan δ. The first is τ_{LF} (ms) ascribed to surface water presumably accumulated right below the pore/material interface. The next is τ_{MF} and τ_{HF} (both in μs) ascribed to water-free materials.

Author contributions

Tosapol Maluangnont: conceptualization; writing, review, and editing; funding acquisition; and project administration. Phieraya Pulphol, Satana Pongampai, and Thawanrat Kobkeatthawin: investigation. Siwaporn Meejoo Smith and Naratip Vittayakorn: supervision. All authors have reviewed and approved of the manuscript.

Conflicts of interest

There are no conflicts of interest to declare.

Acknowledgements

References

1 F. Fina, S. K. Callear, G. M. Carins and J. T. S. Irvine, Structural investigation of graphitic carbon nitride via XRD and neutron diffraction, *Chem. Mater.*, 2015, **27**, 2612–2618.

2 T. Kobkeatthawin, J. Trakulmututa, T. Amornsakchai, P. Kajitvichyanukul and S. M. Smith, Identification of active species in photodegradation of aqueous imidacloprid over g-C$_3$N$_4$/TiO$_2$ Nanocomposites, *Catalysts*, 2022, **12**, 120.

3 X. Wang, X. Chen, A. Thomas, X. Fu and M. Antonietti, Metal-containing carbon nitride compounds: a new

functional organic–metal hybrid material, *Adv. Mater.*, 2009, **21**, 1609–1612.

4 Z. Chen, S. Mitchell, E. Vorobyeva, R. K. Leary, R. Hauert, T. Furnival, Q. M. Ramasse, J. M. Thomas, P. A. Midgley, D. Dontsova, *et al.*, Stabilization of single metal atoms on graphitic carbon nitride, *Adv. Funct. Mater.*, 2017, **27**, 1605785.

5 R. Mohini and N. Lakshminarasimhan, Coupled semiconductor nanocomposite g-C$_3$N$_4$/TiO$_2$ with enhanced visible light photocatalytic activity, *Mater. Res. Bull.*, 2016, **76**, 370–375.

6 X. Wang, S. Blechert and M. Antonietti, Polymeric graphitic carbon nitride for heterogeneous photocatalytsis, *ACS Catal.*, 2012, **2**, 1596–1606.

7 D. J. Martin, K. Qiu, S. A. Shevlin, A. D. Handoko, X. Chen, Z. Guo and J. Tang, Highly efficient photocatalytic H$_2$ evolution from water using visible light and structure-controlled graphitic carbon nitride, *Angew. Chem., Int. Ed.*, 2014, **53**, 9240–9245.

8 Y. Dong, Q. Wang, H. Wu, Y. Chen, C.-H. Lu, Y. Chi and H.-H. Yang, Graphitic carbon nitride materials: sensing, imaging and therapy, *Small*, 2016, **12**, 5376–5393.

9 S. K. Gaddam, R. Pothu and R. Boddula, Graphitic carbon nitride (g-C$_3$N$_4$) reinforced polymer nanocomposite systems—a review, *Polym. Compos.*, 2020, **41**, 430–442.

10 N. Konofaos, C. T. Angelis, E. K. Evangelou, C. A. Dimitriadis and S. Logothetidis, Charge carrier response time in sputtered *a*-C/*n*-Si heterojunctions, *Appl. Phys. Lett.*, 2001, **79**, 2381–2383.

11 C. Godet, J. P. Kleider and A. S. Gudovskikh, Frequency scaling of ac hopping transport in amorphous carbon nitride, *Diamond Relat. Mater.*, 2007, **16**, 1799–1805.

12 J. P. Kleider, A. S. Gudovskikh and C. Godet, DC and AC hopping transport in metal/amorphous carbon nitride/metal devices, *J. Non-Cryst. Solids*, 2006, **352**, 1323–1326.

13 N. Konofaos, E. K. Evangelou, S. Logothetidis and M. Gioti, Electrical properties of carbon nitride films on silicon, *J. Appl. Phys.*, 2002, **91**, 9915–9918.

14 L. M. Zambov, C. Popov, M. F. Plass, A. Bock, M. Jelinek, J. Lancok, K. Masseli and W. Kulisch, Capacitance humidity sensor with carbon nitride detecting element, *Appl. Phys. A*, 2000, **70**, 603–606.

15 Z. Zhang, J. Huang, Q. Yuan and B. Dong, Intercalated graphitic carbon nitride: a fascinating two-dimensional nanomaterial for an ultra-sensitive humidity nanosensor, *Nanoscale*, 2014, **6**, 9250–9256.

16 N. Urakami, K. Ogihara, H. Futamura, K. Takashima and Y. Hashimoto, Demonstration of electronic devices in graphitic carbon nitride crystalline film, *AIP Adv.*, 2021, **11**, 075204.

17 K. Takashima, N. Urakami and Y. Hashimoto, Electronic transport and device application of crystalline graphitic carbon nitride film, *Mater. Lett.*, 2020, **281**, 128600.

18 P. C. Patra and Y. N. Mohapatra, Dielectric constant of thin film graphitic carbon nitride (g-C$_3$N$_4$) and double dielectric Al$_2$O$_3$/g-C$_3$N$_4$, *Appl. Phys. Lett.*, 2021, **118**, 103501.

19 P. C. Patra and Y. N. Mohapatra, Graphitic carbon nitride (g-C$_3$N$_4$)/Al$_2$O$_3$ heterostructure as double dielectric: a comparative study in MIS based on a-IGZO, *IEEE J. Electron Devices Soc.*, 2021, **9**, 618–622.

20 M. Aono and S. Nitta, High resistivity and low dielectric constant amorphous carbon nitride films: application to low-k materials for ULSI, *Diamond Relat. Mater.*, 2002, **11**, 1219–1222.

21 Y. Noda, C. Merschjann, J. Tarábek, P. Amsalem, N. Koch and M. J. Bojdys, Directional charge transport in layered two-dimensional triazine-based graphitic carbon nitride, *Angew. Chem., Int. Ed.*, 2019, **58**, 9394–9398.

22 X. Guo, D. Kuang, Z. Zhu, Y. Ding, L. Ge, Z. Wu, B. Du, C. Liang, G. Meng and Y. He, Humidity sensing by graphitic carbon nitride nanosheet/TiO$_2$ nanoparticle/Ti$_3$C$_2$T$_x$ nanosheet composites for monitoring respiration and evaluating the waxing of fruits, *ACS Appl. Nano. Mater.*, 2021, **4**, 11159–11167.

23 S. Pareek, M. Sharma, S. Lai and J. K. Quamara, Polymeric graphitic carbon nitride-barium titanate nanocomposites with different content ratios: a comparative investigation on dielectric and optical properties, *J. Mater. Sci.: Mater. Electron.*, 2018, **29**, 13043–13051.

24 S. Pareek and J. K. Quamara, Dielectric and optical properties of graphitic carbon nitride-titanium dioxide nanocomposite with enhanced charge separation, *J. Mater. Sci.*, 2018, **53**, 604–612.

25 S. Liu, T. Ye, Y. Liu, H. Cheng and X. Liu, Graphitic-carbon nitride nanosheets as a new inorganic filler for improving energy storage density of PVDF-based dielectric composites, *J. Mater. Sci.: Mater. Electron.*, 2020, **31**, 13063–13069.

26 R. Ratshiedana, A. T. Kuvarega and A. K. Mishra, Titanium dioxide and graphitic carbon nitride-based nanocomposites and nanofibers for the degradation of organic pollutants in water: a review, *Environ. Sci. Pollut. Res.*, 2021, **28**, 10357–10374.

27 Y. Xiao, S. Guo, G. Tian, B. Jiang, Z. Ren, C. Tian, W. Li and H. Fu, Synergistic enhancement of surface reactions and charge separation over holey C$_3$N$_4$/TiO$_2$ 2D heterojunctions, *Sci. Bull.*, 2021, **66**, 275–283.

28 Y. Meng, J. Gao, Z. Zhao, J. Amoroso, J. Tong and K. S. Brinkman, Review: recent progress in low-temperature proton-conducting ceramics, *J. Mater. Sci.*, 2019, **54**, 9291–9312.

29 V. Bugris, H. Haspel, Á. Kukovecz, Z. Kónya, M. Sipiczki, P. Sipos and I. Pálinkó, Water types and their relaxation behavior in partially rehydrated CaFe-mixed binary oxide obtained from CaFe-layered double hydroxide in the 155–298 K temperature range, *Langmuir*, 2013, **29**, 13315–13321.

30 H. Haspel, V. Bugris and Á. Kukovecz, Water sorption induced dielectric changes in titanate nanowires, *J. Phys. Chem. C*, 2013, **117**, 16686–16697.

31 W. Hu, L. Li, W. Tong and G. Li, Water-titanate intercalated nanotubes: Fabrication, polarization, and giant dielectric property, *Phys. Chem. Chem. Phys.*, 2010, **12**, 12638–12646.

32 Š. Csáki, J. Ondruška, V. Trnovcová, I. Štubňa, P. Dobroň and L. Vozár, Temperature dependence of the AC conductivity of illitic clay, *Appl. Clay Sci.*, 2018, **157**, 19–23.

33 X. Kang, A. Chatzitakis, T. Aarholt, X. Sun, C. Negri and T. Norby, Facet-engineered TiO_2 nanomaterials reveal the role of water-oxide interactions in surface protonic conduction, *J. Mater. Chem. A*, 2022, **10**, 218–227.

34 G. Garcia-Belmonte, V. Kytin, T. Dittrich and J. Bisquert, Effect of humidity on the ac conductivity of nanoporous TiO_2, *J. Appl. Phys.*, 2003, **94**, 5261–5264.

35 H.-Z. Wu, L.-M. Liu and S.-J. Zhao, The role of the defect on the adsorption and dissociation of water on graphitic carbon nitride, *Appl. Surf. Sci.*, 2015, **358**, 363–369.

36 H.-Z. Wu, L.-M. Liu and S.-J. Zhao, The effect of water on the structural, electronic and photocatalytic properties of graphitic carbon nitride, *Phys. Chem. Chem. Phys.*, 2014, **16**, 3299–3304.

37 W. Meng, S. Wu, X. Wang and D. Zhang, High-sensitivity resistive humidity sensor based on graphitic carbon nitride nanosheets and its application, *Sens. Actuators, B*, 2020, **315**, 128058.

38 Z. Yan, C. Wang, R. Yu, Z. Hu and L. Xiao, Graphitic carbon nitride for enhancing humidity sensing of microfibers, *J. Lightwave Technol.*, 2021, **39**, 3896–3902.

39 Y.-C. Yeh, T.-Y. Tseng and D.-A. Chang, Electrical properties of porous titania ceramic humidity sensors, *J. Am. Ceram. Soc.*, 1989, **72**, 1472–1475.

40 J. T. S. Irvine, D. C. Sinclair and A. R. West, Electroceramics: characterization by impedance spectroscopy, *Adv. Mater.*, 1990, **2**, 132–138.

41 R. Gerhardt, Impedance and dielectric spectroscopy revisited: distinguishing localized relaxation from long-range conductivity, *J. Phys. Chem. Solids*, 1994, **55**, 1491–1506.

42 S. Sriphan, P. Pulphol, T. Charoonsuk, T. Maluangnont and N. Vittayakorn, Effect of adsorbed water and temperature on the universal power law behavior of lepidocrocite-type alkali titanate ceramics, *J. Phys. Chem. C*, 2021, **125**, 12910–12920.

43 A. K. Jonscher, Dielectric relaxation in solids, *J. Phys. D: Appl. Phys.*, 1999, **32**, R57–R70.

44 A. K. Jonscher, The 'universal' dielectric response, *Nature*, 1977, **267**, 673–679.

45 M. D. Donohue and G. L. Aranovich, Classification of Gibbs adsorption isotherms, *Adv. Colloid Interface Sci.*, 1988, **76–77**, 137–152.

46 P. Zhang, Y. Tong, Y. Liu, J. J. M. Vequizo, H. Sun, C. Yang, A. Yamakata, F. Fan, W. Lin, X. Wang, *et al.*, Heteroatom dopants promote two-electron O_2 reduction for photocatalytic production of H_2O_2 on polymeric carbon nitride, *Angew. Chem., Int. Ed.*, 2020, **59**, 16209–16217.

47 W. Li, Z. Guo, L. Jiang, L. Zhong, G. Li, J. Zhang, K. Fan, S. Gonzalez-Cortes, K. Jin, C. Xu, *et al.*, Facile in situ reductive synthesis of both nitrogen deficient and protonated g-C_3N_4 nanosheets for the synergistic enhancement of visible-light H_2 evolution, *Chem. Sci.*, 2020, **11**, 2716–2728.

48 R. Guo, D. Zeng, Y. Xie, Y. Ling, D. Zhou, L. Jiang, W. Jiao, J. Zhao and S. Li, Carbon nitride quantum dots (CNQDs)/ TiO_2 nanoparticle heterojunction photocatalysts for enhanced ultraviolet-visible-light-driven bisphenol a degradation and H_2 production, *Int. J. Hydrogen Energy*, 2020, **45**, 22534–22544.

49 D. Vidyasagar, A. Balapure, S. G. Ghugal, A. G. Shende and S. S. Umare, Template-free macro-mesoporous TiO_2/carbon nitride interface for visible-light-driven photocatalysis, *Phys. Status Solidi A*, 2019, **216**, 1900212.

50 M. Lazzeri, A. Vittadini and A. Selloni, Structure and energetics of stoichiometric TiO_2 anatase surfaces, *Phys. Rev. B*, 2001, **63**, 155409.

51 B. Zhu, B. Cheng, L. Zhang and J. Yu, Review on DFT calculation of s-triazine-based carbon nitride, *Carbon Energy*, 2019, **1**, 32–56.

52 K. Gelin, A. Bodin, P. Gatenholm, A. Mihranya, K. Edwards and M. Strømme, Characterization of water in bacterial cellulose using dielectric spectroscopy and electron microscopy, *Polymer*, 2007, **48**, 7623–7631.

53 T. Charoonsuk, S. Sriphan, P. Pulphol, W. Vittayakorn, N. Vittayakorn and T. Maluangnont, AC conductivity and dielectric properties of lepidocrocite-type alkali titanate tunable by interlayer cation and intralayer metal, *Inorg. Chem.*, 2020, **59**, 15813–15823.

54 T. Maluangnont, S. Sriphan, T. Charoonsuk and N. Vittayakorn, Dielectric spectroscopy and electric modulus analyses of $Ti_{0.8}O_2$ nanosheets-Ag nanoparticles-cellulose filter paper composites, *Integr. Ferroelectr.*, 2022, **224**, 214–224.

55 J. C. Dyre, P. Maass, B. Roling and D. L. Sidebottom, Fundamental questions relating to ion conduction in disordered solids, *Rep. Prog. Phys.*, 2009, **72**, 046501.

56 D. L. Sidebottom, Dimensionality dependence of the conductivity dispersion in ionic materials, *Phys. Rev. Lett.*, 1999, **83**, 983–986.

57 M. Liu, J. K. Beattie and A. Gray-Weale, The surface relaxation of water, *J. Phys. Chem. B*, 2012, **116**, 8981–8988.

58 S. T. van der Post, C.-S. Hsieh, M. Okuno, Y. Nagata, H. J. Bakker, M. Bonn and J. Hunger, Strong frequency dependence of vibrational relaxation in bulk and surface water reveals sub-picosecond structural heterogeneity, *Nat. Commun.*, 2015, **6**, 8384.